

Growth of electromigration-induced hillocks in Al interconnects

J.A. Nucci, A. Straub, E. Bischoff, E. Arzt, and C.A. Volkert^{a)}

Max-Planck-Institut für Metallforschung, Heisenbergstraße 3, D-70569 Stuttgart, Germany

(Received 6 June 2002; accepted 5 August 2002)

Electromigration-induced hillock growth in polycrystalline Al segments was extensively investigated. Hillocks composed of columnar grains grew near the anode by epitaxial Al addition at the interface between the Al and underlying TiN layer, which pushed up the original Al film. The hillocks rotated away from their initial (111) out-of-plane orientation in a manner consistent with the physical rotation of the hillock surface. Wedgelike and rounded hillocks were observed, and their formation is explained by the interaction between grain extrusion and grain growth. Trends elucidated by review of both thermal- and electromigration-induced hillock studies can be explained by the mechanisms identified in this work.

I. INTRODUCTION

Passing current through an interconnect generates a net flux of atoms, typically in the direction of the electron flow, which is called electromigration. Divergences in this current-induced atom flux lead to regions of atom accumulation and depletion, which in turn lead to the local generation of mechanical stresses. Particularly large stresses are created at interconnect segment ends, and it is generally accepted that voids result from tensile stresses generated at the cathode end while whiskers, and more commonly, hillocks, form in response to compressive stresses generated at the anode end. If these stresses exceed a critical value,¹ the resulting damage can lead to the electrical failure of interconnects.

Hillocks and voids that compromise metallization reliability can also form as a result of the thermal stresses generated by annealing a metal film or line that is rigidly attached to a silicon substrate. Since the thermal expansion coefficient of the metal greatly exceeds that of the silicon, heating induces compressive stresses and thermal hillock formation while cooling induces tensile stresses and stress-induced void formation.

Both electromigration- and thermal-induced hillocks in Al lines and films have been studied and their morphologies and crystallographic orientations have been reported in literature. At the early stages of electromigration testing and after annealing, whiskers and fairly simple shapes, such as rounded^{2–8} and wedge-shaped hillocks^{4–6,9} have been reported. Hillocks with flat surfaces inclined to the film surface^{5,9–11} as well as those with terraced surfaces⁷ have also been reported. For all morphologies, the hillocks consist of either a single grain

or multiple grains and no voids or pores were found underneath them. However, only thermal annealing produces round hillocks surrounded by thin grooved regions or moats,^{4,9} which are believed to result from tensile stress relaxation during cooling. Electromigration-induced hillocks that appear extruded^{10–13} are likely the early stages of whisker formation. At the later stages of electromigration testing, the hillocks are larger and exhibit more complex and fanciful shapes.¹³ Since electromigration involves longer range atom transport than occurs during thermal cycling, it is not surprising that electromigration-induced hillocks tend to be larger than thermal hillocks.

Both electromigration- and thermal-induced hillocks either nucleate as new, randomly oriented grains at grain boundaries or triple points located on top of the Al film^{3,5,6,14,15} or they grow from the lower Al interface,^{2,8,10,11} which can occur epitaxially.^{2,10} In both cases, the crystallographic orientations of the grains composing the hillocks deviates considerably from the (111) out-of-plane texture typical of the surrounding grains.^{3,4,7,14,15}

Links between hillock growth and lateral grain growth have been identified for both thermal and electromigration-induced hillocks. Gladkikh *et al.* found that electromigration-induced hillock growth was associated with grain boundary migration where the hillock border coincided with the moving boundary.¹² Several studies, including this one, revealed that grain boundaries bordering hillocks often tilted.^{9,12} In a recent article by Kim *et al.*, grain boundary migration was shown to enhance thermal hillock formation by at least a factor of four.¹⁶

Formation and growth mechanisms for hillocks are a function of the active diffusion pathways and both the availability and efficiency of these pathways depend on the sample fabrication, geometry, and microstructure. Thus, it is not surprising that various mechanisms,

^{a)}Address all correspondence to this author.
e-mail: volkert@mf.mpg.de

such as grain boundary diffusion,^{4,6,17} coupled grain boundary sliding and interface diffusion,¹⁸ coupled grain boundary diffusion and surface diffusion,^{9,19} dislocation creep,⁴ and Nabarro-Herring creep,²⁰ have all been proposed to explain hillock formation and growth in thin metal films and interconnects.

In this paper, we thoroughly examine electromigration-induced hillock formation in unpassivated, polycrystalline aluminum interconnects. The goal of this study is to elucidate which mechanisms contribute to and control the hillock formation process. It will be argued that subtle differences in the relative importance of the different mechanisms can lead to very different hillock morphologies as well as to different values of the critical stress for electromigration-induced damage formation.

II. EXPERIMENTAL

The structures used for electromigration testing consisted of 10- μm -wide Al segments of various lengths (from 6 to 26 μm) on a continuous 10- μm -wide TiN/Ti runner. They were fabricated from films of Ti (45 nm thick), TiN (200 nm thick), and pure Al (100, 200, 400, 600, or 800 nm thick), which were sputter deposited onto oxidized (100)Si wafers at 225 °C and then patterned into electromigration test structures using electron beam lithography in a scanning electron microscope (SEM) and reactive ion etching. After fabrication, the structures were annealed in air at 400 °C for 1 h to stabilize the grain structure. The samples were then electromigration tested in a needle probe station at 225 °C in air using a current density of 1 MA/cm² for 4 to 50 h.

The sample microstructure and electromigration damage were characterized using a number of methods. Focused ion beam (FIB) microscopy with a 30 keV Ga beam was used to image the Al grain structure and to cut cross sections through both undamaged segments and hillocks. The cross sections were subsequently imaged in the FIB or in a field emission scanning electron microscope (FESEM) at 3 keV. The FESEM was also used to closely examine hillock morphology during periodic interruptions of electromigration testing. Atomic force microscopy (AFM) was used to study the hillock morphology and surface structure after testing was completed. The AFM was run in tapping mode with a 5–10-nm-radius, 10–15- μm -high, etched silicon tip.

Global texture data was collected on unpatterned films by θ -2 θ x-ray scans in a diffractometer. Localized crystallographic information within segments was gathered using Electron backscatter diffraction (EBSD) in a SEM. Grain and hillock orientations were monitored by manual EBSD measurements taken from selected locations both before electromigration testing and during periodic interruptions of electromigration tests. The EBSD determined orientations are accurate to approximately 1°.

Transmission electron microscopy (TEM) cross-sectional samples of electromigration hillocks were prepared using the FIB. A tungsten layer was initially deposited on the sample surface in the FIB as protection from further Ga ion beam damage. TEM lamellae approximately 20 μm long \times 4 μm high \times 250 nm thick were cut from the desired region of the sample. The lamellae were then transferred onto a TEM grid using a micromanipulator under an optical microscope. The grids were carbon coated to better secure the specimens. Images were obtained using an energy filtering TEM at 120 kV with a LaB6 filament.

III. RESULTS

The as-fabricated Al segments were of uniform width and height and consisted of columnar grains. θ -2 θ x-ray scans of films from which the samples were fabricated showed only a (111) peak, indicating that the films were strongly (111) textured, and rocking curves showed that the (111) direction lay within 5° of the film normal. FIB and TEM cross sections of the samples revealed that small (approximately 100 nm) TiAl₃ precipitates formed at the Al/TiN interface during annealing, probably by reaction of Al with excess Ti in the TiN film. FIB analysis revealed an average grain size slightly larger than the film thickness for the as-deposited films and showed that annealing for 1 h at 400 °C produced grain growth only in the 800-nm-thick films. For example, the as-deposited and annealed 100-nm-thick films had an average grain size of 0.12 μm while the 800-nm-thick films had an average grain size of 1.02 μm in the as-deposited condition and 1.49 μm after annealing.

The FIB images also revealed a network of surface grooves which plainly coincided with the grain boundaries in all but the annealed 800-nm-thick films. From this observation, it is believed that the grooves formed at the grain boundaries during or immediately following deposition and did not move during subsequent annealing since they are replicated in the native oxide layer. Therefore, in all but the 800-nm annealed segments, the grooves marking the grain boundary positions before electromigration testing were used to look for evidence of grain growth during electromigration.

After several hours of electromigration testing at 1 MA/cm², damage was observed in the longer segments, as shown in Fig. 1. In this figure and those that follow, the x direction is along the segment length (direction of current flow) and the y direction is across the segment width. Al depleted from the cathode end of the segments accumulated as hillocks at the anode ends. While hillocks mostly formed at the segment edge, they were also observed as far as 10 μm from the anode. That the shorter segments were not damaged is due to the existence of the well-known “critical length” for

electromigration damage formation.¹ Upon further testing of the structure in Fig. 1, all of the longer segments shortened to roughly the critical length ($13\ \mu\text{m}$ at $1\ \text{MA}/\text{cm}^2$) by cathode depletion, and electromigration stopped. The total hillock volume was larger for longer segments, as expected, since the amount of transported material was also larger. Depletion generally occurred uniformly at the cathode edge accompanied by the thinning of individual grains near the cathode end.²¹ Additional studies that examine the influence of the sample geometry and testing conditions on the critical product for these samples are reported by Straub.²²

Figure 2 shows a FIB microscope image of a hillock formed directly at the anode end of a segment. This sample was first tested at $225\ ^\circ\text{C}$, then $250\ ^\circ\text{C}$, and finally at $275\ ^\circ\text{C}$. Presumably because of a surface reaction, such as Al oxidation or reaction of etch residues, the

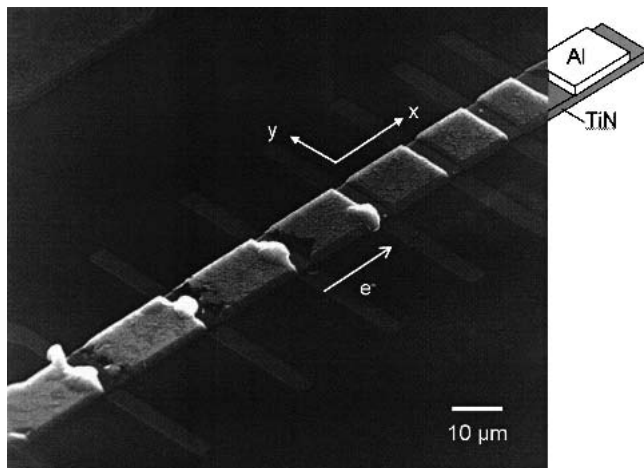


FIG. 1. FIB image of 600-nm-thick Al segments after testing at $1\ \text{MA}/\text{cm}^2$ and $225\ ^\circ\text{C}$ for 50 h.

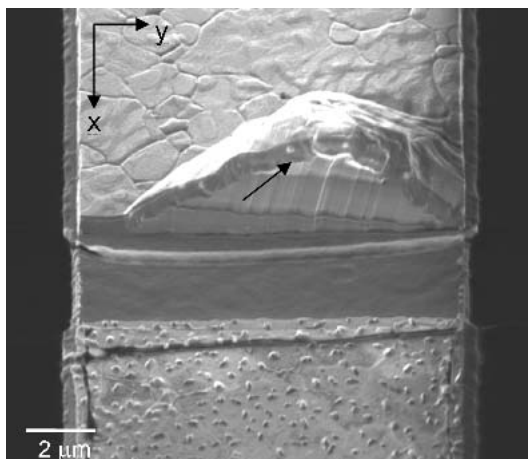


FIG. 2. FIB image of an as-grown hillock formed at the end of a 600-nm-thick Al segment. Material accumulation at the Al/TiN interface pushed up the original Al film (indicated by the arrow). The three layers under the original film were added to the hillock as a result of sequential electromigration testing at 225, 250, and $275\ ^\circ\text{C}$.

material added to the hillock during each temperature interval exhibited a different contrast in the FIB. The top stripe corresponds to the original film thickness, and the next three stripes correspond to the material added at $225\ ^\circ\text{C}$ (second stripe from the top), $250\ ^\circ\text{C}$, and $275\ ^\circ\text{C}$ (bottom stripe). The different contrast stripes reveal the progression of the hillock shape during growth and show that growth proceeded by atom addition at the Al/TiN interface. The cross-sectional FIB image in Fig. 3 provides additional support for hillock growth from the Al/TiN interface; small TiAl_3 particles, which were located all along the Al/TiN interface, were pushed upwards as Al atoms were added to the interface during hillock growth.

Channeling contrast in the FIB also revealed that the atoms are epitaxially added to the growing hillock, as shown in the cross-sectional FIB images in Figs. 3, 4(b) and 5. The hillocks in Figs. 3 and 4 are composed of single grains while the hillock in Fig. 5 is composed of several columnar grains. In general, small hillocks are single grained and larger hillocks are composed of either a single, large grain or a few moderately sized, columnar grains. Often, the grain boundaries bordering the hillocks, such as those in Figs. 3 and 4(b), are tilted away from the hillock. Grain boundaries within undamaged regions are generally vertical.

That hillock growth can be accompanied by lateral grain growth was confirmed by comparing the grain boundary positions with the grooves at the film surface. For example, in Fig. 4, grooves are evident at the hillock surface while the grain boundaries are located at the edge of the hillock, indicating that the grain boundaries moved during hillock formation. However, hillock growth was not always accompanied by grain growth, and no

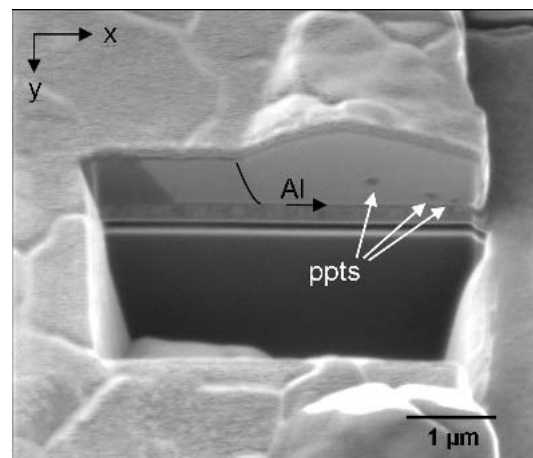


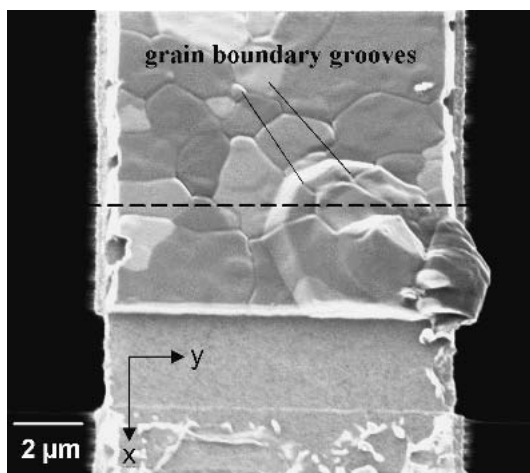
FIG. 3. FIB image of a cut through a hillock in an 800-nm-thick Al segment sectioned along the line length. The original Al/TiN interface is marked by TiAl_3 precipitates, which were pushed up during hillock growth. Since the contrast between the hillock and the adjacent grain is minimal, the boundary between them was drawn in for easier viewing.

evidence of grain growth during electromigration was found in either subcritical length segment, such as in the three shortest segments in Fig. 1, or in undamaged regions of the longer segments. Several FIB observations suggest the possibility of grain growth near depletion sites at the cathode; however the observations are not conclusive.

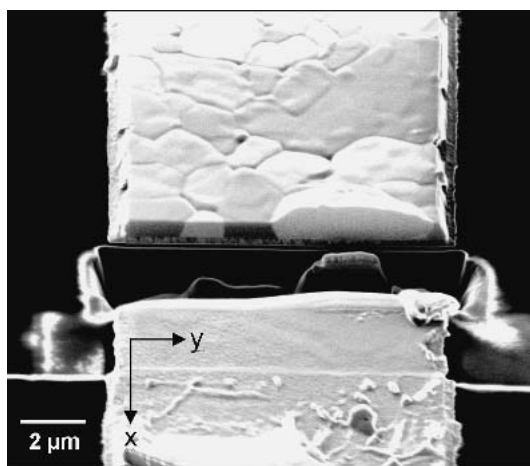
FESEM images of hillocks tested for 10 h or less revealed two distinct growth morphologies that may be correlated to the absence or occurrence of lateral grain boundary motion during hillock growth. Flat-topped, wedge-shaped hillocks appeared to extrude from the segment at a constant angle (Mode I), as shown in Fig. 6. If this flat defines the grain size at hillock formation, then Mode I hillocks grow without lateral grain growth. Other hillocks contained a flat region surrounded by a curved, striated surface (Mode II), as shown in Figs. 7(a) and

8(b). The surrounding, rounded regions of the often larger, Mode II hillocks indicate the extent of lateral grain growth as hillock growth proceeded. Of the 36 hillocks investigated after 10 h of testing or less, 27 (75%) showed evidence of lateral hillock growth. Hillocks tested for longer times displayed more varied morphologies ranging from simple, rounded hillocks, as in Figs. 2 and 5, to more unusual shapes, as shown in Figs. 1 and 4.

The surface of the hillock shown in Fig. 7(a) was carefully examined by AFM. Figure 7(b) shows an AFM image of this hillock surface, and Fig. 7(c) contains a line scan across part of this region. The striations always lie perpendicular to the apparent growth direction and result from 5- to 10-nm-high steps on the sample surface. They are not consistent with the appearance of surface slip bands, since one would expect a series of roughly



(a)



(b)

FIG. 4. FIB images of an electromigration-induced hillock in a 600-nm-thick film. (a) Grooves on the film surface mark the original grain boundary locations. (b) A cross section through the hillock shows that lateral grain growth accompanied hillock growth. Grain growth did not occur in the undamaged regions of the interconnect.

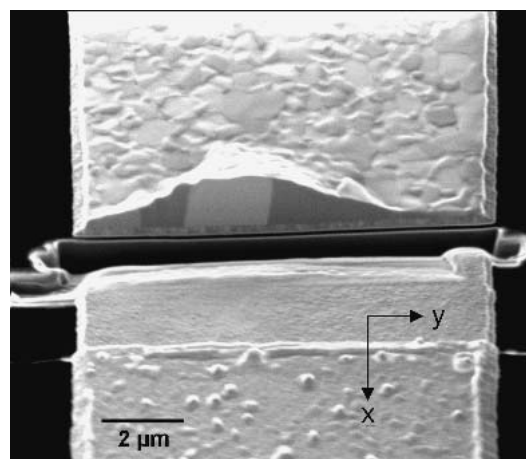


FIG. 5. FIB cross section showing a hillock composed of several columnar grains.

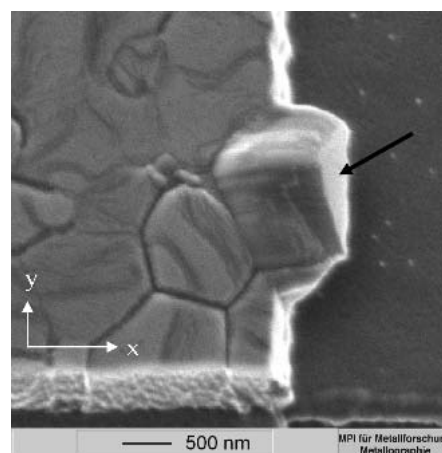
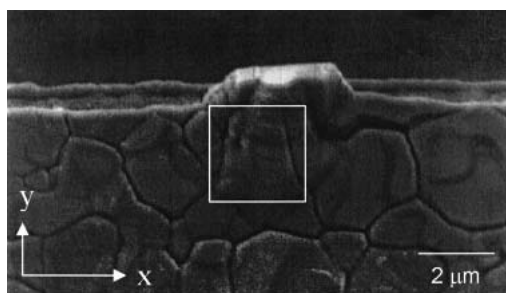


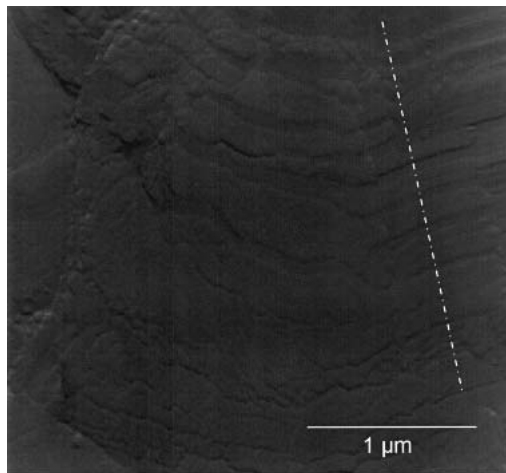
FIG. 6. SEM micrograph of a flat-topped, wedge-shaped hillock in an 800-nm-thick film after 10 h of electromigration testing. The flat, which is indicated by the arrow, is part of the original Al surface, and the grain appears to have extruded from the film without accompanying lateral grain growth.

straight, parallel steps resulting from slip activity on the plane with the highest Schmid factor. However, they are consistent with fracture of the native oxide, which has a thickness of approximately 7 nm, based upon Auger depth profiles for oxygen.

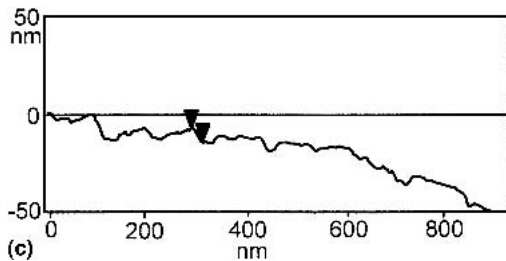
Several hillocks were cross sectioned using the FIB and investigated in the TEM. The samples were examined using two beam conditions at damaged and intact regions of the line for better observation of dislocations. Similar low dislocation densities of approximately $10^{13}/\text{m}^2$ were measured in both regions. No evidence of activated slip systems was found.



(a)



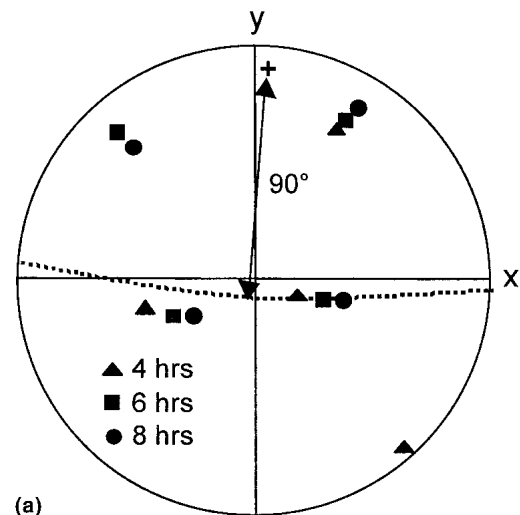
(b)



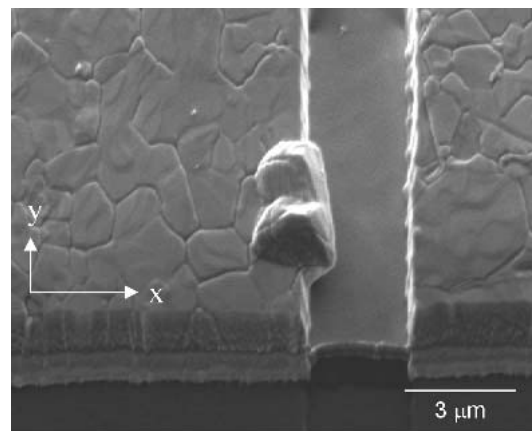
(c)

FIG. 7. (a) SEM micrograph of a hillock formed at the line edge. (b) AFM image of the region corresponding to the white box in (a). The fine surface structure appears to result from fracture of the overlying native oxide layer as the hillock grows. The dashed line denotes the direction of the AFM line scan shown in (c), which reveals 5–10 nm step heights, consistent with the native oxide thickness. The arrows denote a 6.4-nm-high step.

The crystallographic orientations of the hillocks during electromigration were examined using EBSD. Mapping the anode ends of several segments prior to electron microscope testing revealed predominantly (111) textured grains, consistent with the x-ray diffraction results. However, EBSD analysis performed during periodic interruptions of electromigration testing often showed clear rotations in hillock orientation. In general, the hillocks that grew by pure extrusion (Mode I) showed no evidence of crystallographic rotation, presumably after an initial rotation, whereas those which were accompanied by lateral extension (Mode II) rotated away from a (111) out-of-plane orientation during growth. For example, a (111) pole figure in Fig. 8(a) shows crystallographic orientations of the lower hillock in Fig. 8(b), measured after 4, 6, and 8 h of electromigration testing. The (111) direction of the hillock rotated away from its original,



(a)



(b)

FIG. 8. (a) (111) pole figure for a hillock whose orientation was measured after 4, 6, and 8 h of electromigration testing. The dashed great circle denotes the plane in which the hillock normal rotates. The corresponding rotation axis, roughly parallel to the y axis of the line, is shown as the cross in the pole figure. (b) The SEM image for this hillock shows a rigid body rotation about roughly the same axis.

approximately out-of-plane orientation about an axis parallel to the segment end. SEM images and AFM scans of several hillock surfaces confirmed that the normal to the flat region of the hillock surface often rotated in the same direction and by roughly the same amount as the (111) crystallographic direction.

IV. DISCUSSION

The local accumulation of Al to form electromigration-induced hillocks requires the relatively long range transport of atoms. Grain boundaries are the dominant diffusion path in polycrystalline Al lines at typical electromigration testing temperatures. In a study on bamboo segments patterned from the same films as used in this study, diffusion along the Al/TiN interface was shown to be somewhat slower than grain boundary diffusion, and lattice diffusion and dislocation core diffusion were ruled out¹⁰ as contributing to damage formation. Thus, it is concluded that the Al in these polycrystalline segments is likely transported from one end of the segment to the other along grain boundaries. Since the interface between pure Al and its native oxide is known to be a poor diffusion path,¹⁷ the Al/TiN interface is most likely the main diffusion pathway for the bamboo segments manufactured from the same film stack. The Al/TiN interface may also contribute to shorter range transport in the polycrystalline samples.

Given the stress gradient induced by electromigration,^{23,24,25} it is not surprising that depletion occurs at the cathode end and hillocks form near the anode end of the segments. That compressive stress is relieved by hillock formation, rather than uniform thickening of the film, is shown to be energetically favorable except for very small film stresses.¹⁸ The fact that hillocks are occasionally observed as far as 10 μm from the anode is presumably due to local variations in the stress created by microstructural-induced divergences in the electromigration flux. These local variations in the stress are superimposed on the macroscopic stress gradient along the segment and presumably determine the specific sites for hillock formation. The source of these flux divergences is a combination of the variations in grain boundary diffusivity due to misorientations between adjacent grains²⁶ and the component of the electric current along the grain boundary. Although the film is (111) textured, the deviations from perfect (111) out-of-plane texture and the random in-plane texture are sufficient to expect variations in grain boundary diffusivities approaching those of random grain boundaries.

During electromigration, atoms are transported along the grain boundaries and presumably accumulate in the grain boundaries at the anode end of the segment. The fact that material is added to the growing hillocks at the

bottom Al/TiN interface indicates that Al atoms are somehow transported from the grain boundaries into this interface and added to the growing hillock. Lattice and pipe diffusion are too slow to account for this transport. This leaves two possible mechanisms: combined grain boundary and interface diffusion¹⁸ or the glide of dislocations from the grain boundaries to the Al/TiN interface, where they are then annihilated.²⁷

If the stresses generated by transport of atoms along the grain boundaries were relieved by atomic diffusion from the grain boundaries directly into the Al/TiN interface, it is expected that the flux of atoms into the Al/TiN interface would be largest where the normal compressive stresses in the grain boundaries are largest. However, there must be some threshold for addition and removal of atoms from this interface, otherwise stresses in Al films would relax to zero. It is generally known that Al films sustain stresses at elevated temperatures over extended periods of time, and this was verified specifically for the films used in this study using wafer curvature measurements.

It is possible, although less likely, that dislocation glide may be responsible for the observed hillock growth process. Once sufficient stresses had been generated at the anode end, dislocation glide would occur and lead to a shape change of the grain. However, TEM revealed similar, low dislocation densities in both damaged and undamaged regions. Considerable dislocation activity would be necessary to account for the large strains required for hillock growth and it is reasonable to expect that slip planes or glide bands would be observed there. However, no evidence of slip planes was seen in the TEM images or from AFM of the hillock surface. Also, the observed crystallographic rotations of grains during hillock growth are not consistent with those predicted by dislocation glide in single crystals deformed in constrained geometries.²⁸

Once atoms find their way to the Al/TiN interface, likely by combined grain boundary and interface diffusion, they are epitaxially added to an Al grain, generating stresses normal to the interface, as well as stresses in the overlying oxide. These stresses can be relieved by grain boundary sliding and fracture of the native oxide, which leads to the formation of small, often wedge-like extruded regions such as the Mode I hillocks observed in this study. If atoms are nonuniformly added to the bottom interface, then the hillocks would crystallographically and physically rotate as they grow, as shown schematically in Fig. 9(b). The anode end of the line before hillock formation is shown for comparison in Fig. 9(a). If lateral growth of the grain composing the hillock occurs simultaneously, then the combination of extrusion and grain growth can lead to the formation of rounded hillocks. The small, discrete steps observed on the rounded hillock surfaces may result

from a repeated process of grain boundary sliding and accompanying native oxide fracture above the grain boundary followed by grain boundary migration, as depicted in Fig. 9(c). This picture is consistent with AFM observations of the hillock surfaces. If atoms are added under several grains, then multigrain hillocks may form, with or without accompanying grain growth. It is difficult to visualize the formation of rounded hillocks from a single grain without simultaneous grain growth, since the necessary deformation of the overlying film would lead to nonuniform rotations and to subgrain formation, for which there is no evidence in this study.

Hillock growth was accompanied by grain growth for the majority of hillocks studied, and grain growth may be caused by a number of factors. Hillock formation likely reduces local stresses in the grains composing the hillock, which creates a chemical potential driving force for growth of these grains at the expense of their more highly stressed neighbors.²⁹ It has also been argued that the grain boundaries will be pushed ahead of the

advancing hillock area to keep the total grain boundary area as small as possible.³⁰ However, this idea is not consistent with the fact that many of the grain boundaries at the edge of hillocks are inclined [See Figs. 3 and 4(b)] since a vertical grain boundary has a smaller area than an inclined boundary.

It is easy to imagine that changes in the relative importance of the possible diffusive pathways can lead to different hillock formation mechanisms and morphologies. In particular, if interface diffusion is very slow or the incorporation of atoms at the bottom and top interfaces is effectively turned off, then excess atoms accumulated in the grain boundaries have no place to go to relieve the stresses. It is reasonable to expect that the overlying native oxide may fracture above a grain boundary or a triple line and Al may extrude out to form a hillock on top of the original film. This is exactly the hillock morphology observed in both thermal and electromigration hillock studies of Al films deposited directly on SiO₂. In contrast, in many samples with an underlying Al/refractory metal interface, both electromigration- and thermal-induced hillocks often form by material addition at this interface, which is presumably a more efficient diffusion pathway than the Al/SiO₂ interface. While most thermal hillock studies were conducted on Al films deposited directly onto oxide, most electromigration studies were performed on Al deposited onto a refractory metal layer. However, the trend of hillock formation from the upper or lower Al interface likely depends more upon the Al interfaces present than on the nature of the induced stress. As further evidence of the importance of the Al interfaces, another study showed that changing the upper interface from Al/Al₂O₃ to a pure Al surface changed the dominant stress relaxation mechanism altogether.¹⁷ When ultrahigh vacuum (UHV) fabrication and *in situ* thermal cycling were used to suppress native oxide formation, grain boundary compressive stresses were relieved by Al diffusion out of the grain boundaries and onto the sample surface. The same films annealed under non-UHV conditions formed hillocks.

The correlation between hillock shape and grain growth is supported by other studies of hillocks. Rounded, often single-grained hillocks bounded by inclined grain boundaries have also been reported in the literature when hillock growth and grain boundary motion occurred simultaneously.^{9,12} Wedge-shaped hillock formation in the absence of lateral grain growth has been reported by Wang *et al.*⁴ for a 0.1- μm -grain size film, in which the grain boundaries were pinned by oxygen impurities. Thermal cycling of these films deposited on TiN produced hillocks consisting of approximately 200 grains, and the Al was added epitaxially to each grain from the Al/TiN interface. Despite the differences in film composition and grain size between the samples

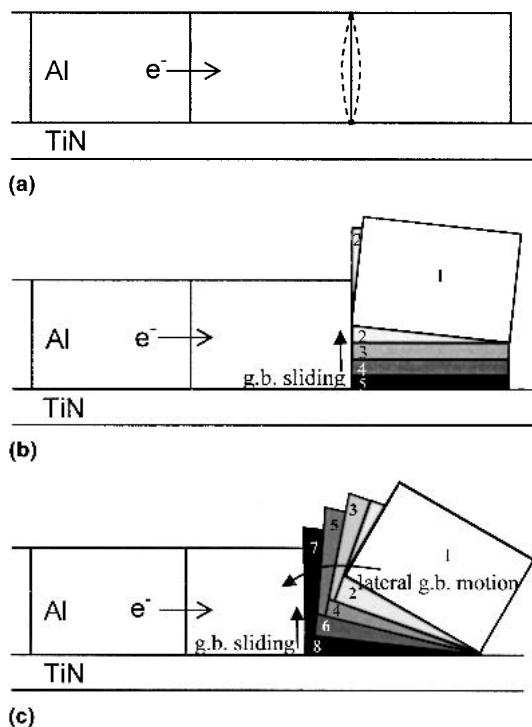


FIG. 9. (a) Schematic diagram of three grains at the anode end of an Al interconnect segment. The dashed lines represent the build-up of compressive stresses at the grain boundary prior to hillock formation. (b) Schematic diagram of Mode I hillock growth. The original grain, labeled 1, is initially rotated (step 2) and then extruded at constant angle without lateral grain growth (steps 3–5) as a result of uniform Al addition at the Al/TiN interface and grain boundary sliding. (c) Schematic diagram of Mode II hillock growth. The original grain forms a rounded hillock by an iterative process of nonuniform Al addition at the Al/TiN interface, grain boundary sliding (even numbered steps), and lateral grain boundary motion (odd numbered steps).

used for this study and Wang's, the processes of epitaxial hillock growth without lateral grain growth produced wedge-shaped hillocks in both cases.

The mechanisms and processes involved in hillock formation may be the same ones that determine the critical stress for damage formation during electromigration. The magnitude of this critical stress is approximately 200 MPa.²⁵ It is tempting to attribute the critical stress to dislocation glide, since extensive modeling of thin films during thermal cycling has attributed stresses of this magnitude to the generation or glide of dislocations in the small film dimensions.³¹ Other mechanisms, such as creep and other diffusion controlled processes, have much smaller thresholds. However, the idea that dislocation glide is the controlling mechanism for hillock formation in these lines can be ruled out based on the fact that there is no evidence of slip bands, either in the grains, as determined by TEM, or at their surface, as measured by AFM, and on the fact that the crystallographic rotations of grains during hillock growth are not consistent with those predicted by dislocation glide in single crystals deformed in constrained geometries.²⁸

Given that dislocation activity is likely ruled out, another event with a threshold is necessary to explain the critical stress for hillock formation. One possibility is that atom addition at the Al/TiN interface is difficult and requires that a critical chemical potential or stress be exceeded.³² This would mean that the critical stress for hillock formation would be extremely sensitive to the exact nature of this interface. Another possibility is fracture of the native oxide, which occurs at least once during hillock formation. However, estimates of the fracture stress, based on simple geometric considerations and assuming a grain boundary normal stress of a few hundred MPa, indicate that the fracture stress must be fairly large, on the order of a few GPa. What is clear, in any case, is that just as samples have different hillock morphologies, they will also have different critical stresses for hillock formation.

V. CONCLUSION

Hillock growth in pure Al segments on continuous TiN runners was studied during electromigration. As a result of the careful, periodic observation of the hillock morphology, crystallographic orientation and surface structure during electromigration testing, various processes and mechanisms associated with hillock formation and growth were identified. Under the bias of the electric current, Al atoms are transported by *grain boundary diffusion* toward the anode end of the segment, where compressive stresses normal to grain boundaries are generated. The atoms are then transported from the grain boundaries to the bottom interface, either by *dislocation glide* or more likely, by *combined grain boundary and*

interface diffusion. The *epitaxial Al addition* at the Al/TiN interface under a grain or grains pushes the original material up, leading to *grain boundary sliding, native oxide fracture, and extrusion*. If Al is nonuniformly added at the interface, both *physical and crystallographic rotation* of the hillock occurs about roughly the same axis. The two basic hillock morphologies observed are proposed to result from hillock growth either without, or more commonly with, accompanying lateral *grain growth*. Wedgelike extrusions are alleged to form when the grain boundaries bordering hillocks remain stationary and the grain extrudes at a constant angle by grain boundary sliding. In contrast, rounded hillocks are proposed to form by an iterative process of grain boundary migration and grain boundary sliding. The same hillock shapes would be expected in alloyed Al interconnects, provided the addition of the impurity does not affect the mechanisms involved in hillock growth. All of these mechanisms, with the possible exception of native oxide fracture, are most likely also involved in grain depletion and thinning at the cathode end of segments.

These observations were used to explain trends regarding both electromigration and thermal hillocks and in particular, to reveal the importance of the Al interface character on hillock formation and growth. While these results do not elucidate a single critical event or critical stress necessary for hillock formation they do make clear that the many different hillock morphologies observed for both thermally and electromigration-induced hillocks likely reflect subtle changes in the nature of the various mechanisms involved in hillock formation.

ACKNOWLEDGMENTS

The authors gratefully acknowledge Ilan Blech for valuable technical discussions, Birgit Heiland for TEM sample preparation, Danielle Cantarutti for AFM analysis, and Sabine Kühnemann for FESEM work. This project was partially supported by the Deutsche Forschungsgemeinschaft Leibniz program.

REFERENCES

1. I.A. Blech, *J. Appl. Phys.* **47**, 1203 (1976).
2. H. Mori, H. Okabayashi, and M. Komatsu, *Thin Solid Films* **300**, 25 (1997).
3. A. Buerke, H. Wendrock, T. Koetter, S. Menzel, K. Wetzig, and A.V. Glasow, in *Materials Reliability in Microelectronics IX*, edited by C.A. Volkert, A.H. Verbruggen, and D.D. Brown (Mater. Res. Soc. Symp. Proc. **563**, Warrendale, PA, 1999), p. 109.
4. P. Wang, J. Hwang, A. Chuang, and F-S. Huang, *Thin Solid Films* **358**, 292 (2000).
5. F. Ericson, N. Kristensen, and J-A. Schweitz, *J. Vac. Sci. Technol. B* **9**, 58 (1991).
6. D. Gerth, D. Katzner, and M. Krohn, *Thin Solid Films* **208**, 67 (1992).

7. B.C. Martin, C.J. Tracy, J.W. Mayer, and L.E. Hendrickson, *Thin Solid Films* **271**, 64 (1995).
8. D-K. Kim, B. Heiland, W.D. Nix, E. Arzt, M.D. Deal, and J.D. Plummer, *Thin Solid Films* **371**, 278 (2000).
9. F.Y. Genin and W.J. Siekhaus, *J. Appl. Phys.* **79**, 3561 (1996).
10. J. Böhm, C.A. Volkert, R. Mönig, T.J. Balk, and E. Arzt, *J. Elect. Mater.* **31**, 45 (2002).
11. J. Proost, L. Delaey, J. D'Haen, and K. Maex, *J. Appl. Phys.* **91**, 9108 (2002).
12. A. Gladkikh, Y. Lereah, E. Glickman, M. Karpovsky, A. Palevski, and J. Shubert, *Appl. Phys. Lett.* **66**, 1214 (1995).
13. C. Witt, Ph.D. dissertation, University of Stuttgart, Stuttgart, Germany (2000).
14. H. Takatsuija, K. Tsujimoto, K. Kuroda, and H. Saka, *Thin Solid Films* **343-344**, 461 (1999).
15. R.A. Schwarzer and D. Gerth, *J. Elect. Mater.* **22**, 607 (1993).
16. D-K. Kim, W.D. Nix, R.P. Vinci, M.D. Deal, and J.D. Plummer, *J. Appl. Phys.* **90**, 781 (2001).
17. C.Y. Chang and R.W. Vook, *Thin Solid Films* **228**, 205 (1993).
18. P. Chaudhari, *J. Appl. Phys.* **45**, 4339 (1974).
19. L.M. Klinger, L. Levin, and E.E. Glickman, in *Materials Reliability in Microelectronics V*, edited by A.S. Oates, W.F. Filter, R. Rosenberg, A. Lindsay Greer, and K. Gadepally (Mater. Res. Soc. Symp. Proc. **391**, Pittsburgh, PA, 1995), p. 271.
20. E. Glickman and M. Nathan, *Microel. Eng.* **50**, 329 (2000).
21. R.A. Augur, R.A.M. Wolters, W. Schmidt, A.G. Dirks, and S. Kordic, *J. Appl. Phys.* **79**, 3003 (1996).
22. A. Straub, Ph.D. Dissertation, University of Stuttgart, Stuttgart, Germany (2000).
23. I.A. Blech and C. Herring, *Appl. Phys. Lett.* **29**, 131 (1976).
24. M.A. Korhonen, P. Borgeson, K.N. Tu, and C-Y. Li, *J. Appl. Phys.* **73**, 3790 (1993).
25. P.C. Wang, G.S. Cargill, I.C. Noyan, and C-K. Hu, *Appl. Phys. Lett.* **72**, 1296 (1998).
26. O.V. Kononenko, V.N. Matveev, and D.P. Field, *J. Mater. Res.* **16**, 2124 (2001).
27. M.S. Jackson and C-Y. Li, *Acta. Metall.* **30**, 1993 (1982).
28. R.E. Reed-Hill, *Physical Metallurgy Principles*, 2nd ed. (Litton, Monterey, CA, 1973), p. 195.
29. C.V. Thompson, *J. Mech. Phys. Solids* **44**, 657 (1996).
30. F.Y. Genin, *J. Appl. Phys.* **77**, 5130 (1995).
31. W.D. Nix, *Metall. Trans.* **20A**, 2217 (1989).
32. E. Arzt, M.F. Ashby, and R.A. Verrall, *Acta. Metall.* **31**, 1977 (1983).